2333-942X/18©2018IEEE

Online Autotuning of a Servo Drive

Using Wavelet Fuzzy Neural Networks to Search for the Optimal Bandwidth

by Faa-Jeng Lin, Shih-Gang Chen, Wei-An Yu, and Hsiao-Tse Chou

To achieve the optimal bandwidth at different speed commands, an online autotuning technique using two two-input, one-output wavelet fuzzy neural networks (WFNNs) for interior permanent magnet synchronous motor (IPMSM) servo drives is proposed in this article. First, the dynamic performance analysis of a field-oriented control (FOC) IPMSM servo drive system is studied. Then, two two-input, one-output, four-layer WFNNs are proposed for the online autotuning of the gains of a proportional–integral (PI) speed controller of the servo motor drive to search for the optimal bandwidth without using the information of plant parameters and the characteristics of the servo motor drive.

In addition, the network structure and the convergence analysis of the WFNNs are introduced. Finally, experimentation using the IPMSM servo drive based on a floating-point digital signal processor (DSP) is presented.

Closing in on a Servo Drive System

Since IPMSMs have many attractive characteristics, such as a wide speed-operation range, high power density, and large torque-to-inertia ratio, they have been employed in many industrial applications [1]. However, these motors are also well known for their nonlinear machine parameters due to magnetic saturation, cross-coupling effects, and parameter dependence on temperature [2]. Therefore, high-quality IPMSM servo drives are required for high-performance applications. In addition, the quality of servo drives is usually characterized by performance parameters such as the rise time, bandwidth, and sampling time of the controller.

Furthermore, most servo motor drives use a cascaded control structure with an outer position control loop, an intermediate speed control loop, and an inner current/torque control loop. And the performance of the outer control loop depends on the response time of the current control loop. Therefore, the bandwidth of the current control loop must be designed to be as high as possible [3]. In addition, the bandwidth depends both on plant parameters and the delay times, including sampling, pulsewidth modulation (PWM), filter, and calculation [4]–[5]. Therefore, it is very difficult to quantify the optimal bandwidth of servo motor drives in real applications, and the design of an optimal bandwidth of the speed control loop has not been fully explored [6].

On the other hand, the development of autotuning techniques for the speed control loop, which usually includes identification of plant parameters, searching of the optimal bandwidth, and tuning of the speed controller gains, is necessary in commercial servo motor drives. However, there is still no autotuning technique under development that will search for the optimal bandwidth of servo motor drives without using the information of plant parameters and the characteristics of servo motor drives.

The fuzzy neural network (FNN) possesses the characteristic of fuzzy reasoning in handling uncertain information and the characteristic of artificial neural networks in learning from processes [7]. Moreover, the wavelet neural network (WNN) with reduced network size has the ability of converging quickly with high precision owing to the time–frequency localization properties of wavelets [8]. Because of the aforementioned FNN and WNN

Digital Object Identifier 10.1109/MSMC.2018.2837151
Date of publication: 17 October 2018

advantages, the WFNN has been proposed for some advanced applications [9]–[12]. For instance, a fuzzy wavelet polynomial neural network was proposed to combine the advantages of the polynomial neural network and the WFNN in [12] for the applications of time-series prediction and regression problems.

In this article, an intelligent online autotuning scheme for a PI speed controller using two WFNNs is proposed to search the optimal bandwidth without using the information of plant parameters and the characteristics of the servo motor drives. The envisaged WFNN, which has two inputs and one output, uses the first derivative of a Gaussian function as its membership function. In addition, an IPMSM servo drive system using a 32-b floating-point DSP, TMS320F28075, is developed. From experimentation, it was found that the proposed intelligent control approach can guarantee the optimal bandwidth at different speed commands.

From experimentation, it was found that the proposed intelligent control approach can guarantee the optimal bandwidth at different speed commands.

Transfer Function of the IPMSM Servo Drive

An FOC IPMSM servo drive, including speed control loop, current regulators, voltage decoupling, and coordinate transformation, is shown in Figure 1. In this figure, i_a, i_b, and i_c represent the three phase currents; v_d and v_q represent the d axis and q axis stator voltages; i_d and i_q represent the d axis and q axis stator currents; ω_{rm} represents the mechanical rotor speed; P denotes the number of pole pairs; v_α and v_β represent the voltage components of the IPMSM in the stationary frame; i_α and i_β represent the current components of the IPMSM in the stationary frame; the superscript * represents the reference value; and $e(t)$ is the speed-tracking error. Since the magnetic flux λ_m generated from the permanent magnet of the rotor is fixed in relation to the rotor shaft position θ_{rm}, the flux position θ_{re} can be determined by the shaft-position sensor. Using the FOC mechanism, with $i_d = 0$, the electromagnetic torque T_e is proportional to i_q [13]. In addition, two WFNNs are proposed to tune the PI speed controller online, where the inputs of the WFNN are the speed-tracking error and its derivative. The outputs ΔK_P and ΔK_I are the online incremental values of the proportional and integral gains, respectively.

The speed control model of the IPMSM servo drive system is shown in Figure 2(a). The equation of the PI controller in the time domain is

$$i_q^* = K_P e(t) + K_I \int e(t)\, dt, \tag{1}$$

where K_P and K_I are the proportional and integral gains, respectively. By using the Laplace transform, the transfer function of the PI controller is shown as

$$G_1(s) = K_P \frac{t_i s + 1}{t_i s}, \tag{2}$$

where $t_i = K_P/K_I$. To design the speed controller using pole-zero cancellation, all of the delay times of the speed control loop are combined into an effective delay time $t_{\Sigma D}$ as follows [5]:

$$t_{\Sigma D} = t_{ID} + t_{FD} + t_{SD}, \tag{3}$$

where t_{ID} is the delay time of the current control loop $T_I(s)$, t_{FD} is the first-order delay of the speed filter, and t_{SD} is the delay time owing to the calculation of the speed control loop. Then, the speed control model of the IPMSM drive system can be simplified to Figure 2(b). Moreover, the model of the inverter used in the motor servo drive can be simplified and represented by a first-order system with a gain and a phase delay [5] as

$$G_2(s) = \frac{K_T}{t_{\Sigma D} s + 1}, \tag{4}$$

where K_T is a torque constant. In addition, the controlled plant of the motor drive system can be represented as

$$G_3(s) = \frac{1}{Js + B} = \frac{K_q}{t_q s + 1}, \tag{5}$$

where J is the inertia constant, B is the damping coefficient, $K_q = 1/B$, and $t_q = J/B$. The open-loop transfer function of the system is

$$\begin{aligned} G(s) &= G_1(s) G_2(s) G_3(s) \\ &= K_P \left(\frac{t_i s + 1}{t_i s} \right) \cdot \frac{K_T}{t_{\Sigma D} s + 1} \cdot \frac{K_q}{t_q s + 1} \\ &= \frac{K_P K_T K_q (t_i s + 1)}{t_i s (t_{\Sigma D} s + 1)(t_q s + 1)}. \end{aligned} \tag{6}$$

The PI controller of the speed control loop is designed by using pole-zero cancellation, i.e., $t_i = t_q$. Then, the closed-loop transfer function of the speed control can be represented as

$$\begin{aligned} G_c(s) &= \frac{K_P K_T K_q}{t_i s (t_{\Sigma D} s + 1) + K_P K_T K_q} \\ &= \frac{K_P K_T K_q}{t_i t_{\Sigma D} s^2 + t_i s + K_P K_T K_q} \\ &= \frac{\Omega_n^2}{s^2 + 2\xi \Omega_n s + \Omega_n^2}, \end{aligned} \tag{7}$$

where the undamped natural frequency is denoted by $\Omega_n = \sqrt{K_P K_T K_q / t_i t_{\Sigma D}} = \sqrt{K_I K_T K_q / t_{\Sigma D}}$ and also $\xi = \sqrt{t_i / 4 K_P K_T K_q t_{\Sigma D}} = \sqrt{1/4 K_I K_T K_q t_{\Sigma D}}$. The resulting closed-loop transfer function is a standard second-order transfer function.

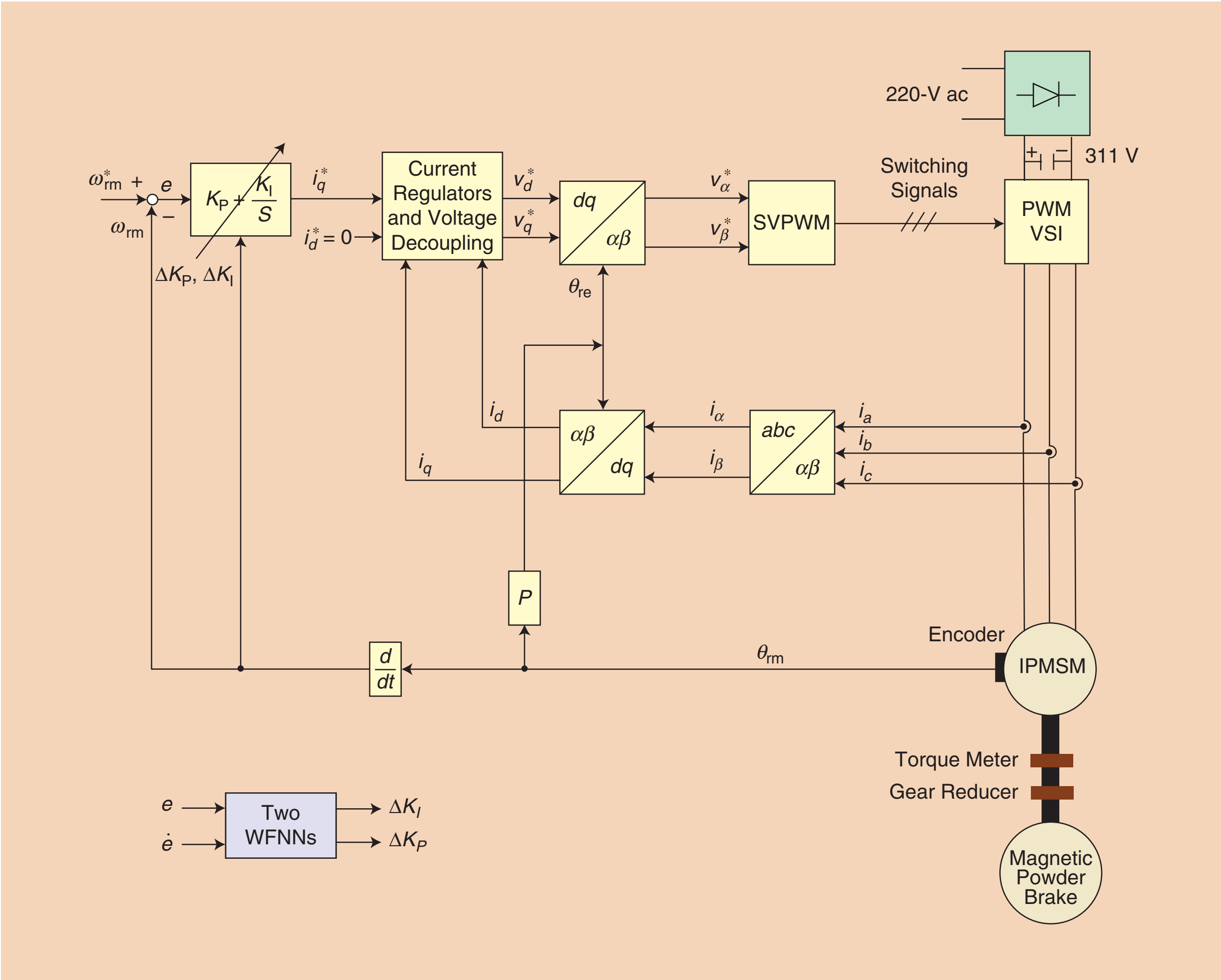

Figure 1. A block diagram of an IPMSM servo drive system. VSI: voltage source inverter; SVPWM: space vector PWM.

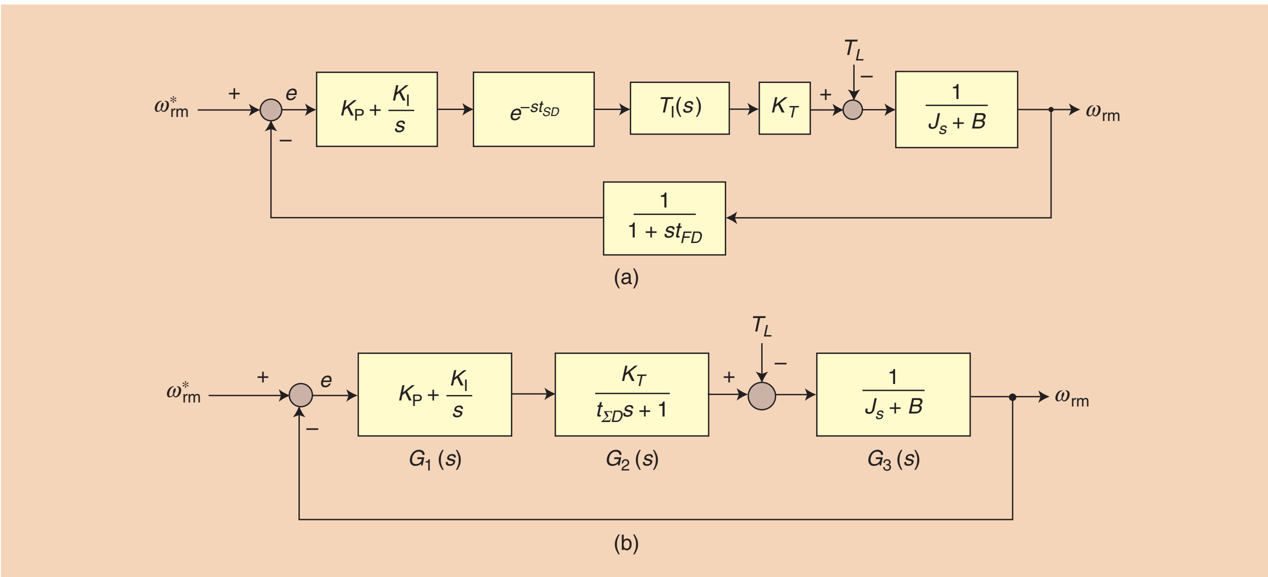

Figure 2. A schematic model of an IPMSM servo drive system: a (a) speed control loop and (b) simplified speed control loop.

Dynamic Performance Analysis of the IPMSM Servo Drive System

According to (7), the closed-loop frequency characteristic of the motor servo drive is expressed in the following:

$$\begin{aligned} G_c(j\Omega) &= \frac{\omega_{rm}(j\Omega)}{\omega^*_{rm}(j\Omega)} \\ &= \frac{\Omega_n^2}{(j\Omega)^2 + 2\xi\Omega_n(j\Omega) + \Omega_n^2}. \\ &= M_B(\Omega)e^{j\phi B(\Omega)} \end{aligned} \tag{8}$$

The cutoff frequency Ω_b is defined as follows:

$$\frac{1}{\sqrt{\left[1-(\Omega_b/\Omega_n)^2\right]^2 + \left[2\xi(\Omega_b/\Omega_n)\right]^2}} \cong 0.707 = \frac{1}{\sqrt{2}}. \tag{9}$$

Then, one can obtain the following relationship among Ω_b, Ω_n, and ξ:

$$\Omega_b = \Omega_n\sqrt{1 - 2\xi^2 + \sqrt{2 - 4\xi^2 + 4\xi^4}}. \tag{10}$$

Since the undamped natural frequency Ω_n is proportional to K_I, from (10), the cutoff frequency Ω_b is also proportional to K_I. That is to say, increasing K_I results in a rise in the cutoff frequency Ω_b. On the other hand, the effect of ξ can be ignored owing to its value being smaller than one.

A Two-Input, Two-Output WFNN

A four-layer WFNN with two inputs and one output, which uses the first derivative of a Gaussian function as its membership function, is shown in Figure 3. The proposed WFNN comprises an input (the i layer), a membership (the j layer), a rule (the k layer), and an output (the o layer).

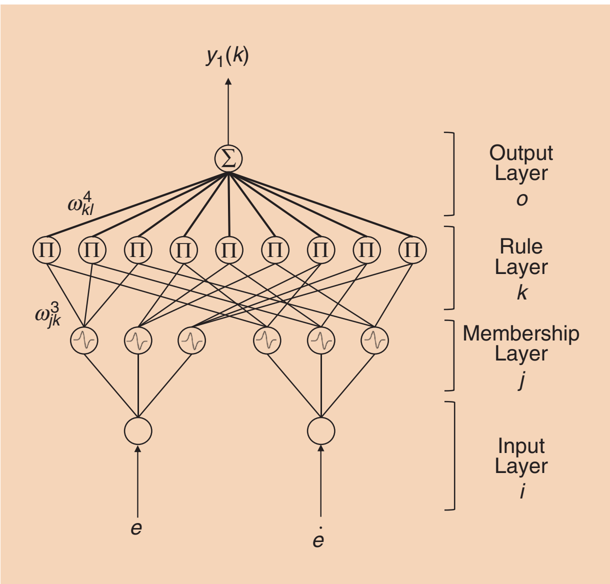

Figure 3. A WFNN with the first derivative of a Gaussian membership function.

In the input layer, the node input and the node output are represented as

$$net_i^1(N) = x_i^1, \quad y_i^1 = f_i^1(net_i^1(N)) = net_i^1(N), \quad i = 1,2, \tag{11}$$

where x_i^1 and y_i^1 denote the input and output of the ith node in this layer, N represents the Nth iteration, and x_1^1 and x_2^1 denote the tracking error e and its derivative $\dot{e}$. Moreover, in the membership layer, each node performs a wavelet from its mother wavelet. The node input and the node output are denoted as

$$net_j^2(N) = \frac{x_i^2 - a_j}{b_j}, \tag{12}$$

$$y_j^2(N) = h(net_j^2(N)), \quad j = 1, 2, 3, \tag{13}$$

$$h(x) = -x\exp(0.5x^2), \tag{14}$$

where a_j and b_j denote the parameters of translation and dilation of the associated wavelet membership function, and x_i^2 and y_j^2 are the input and output of the jth node of the ith input. By properly choosing the parameters in the first derivative of the Gaussian function, it possesses the universal approximation property [14]. Furthermore, in the rule layer, each node k is denoted by Π, which multiplies the input signals and outputs the result of the product. For the kth rule node,

$$\begin{aligned} &net_k^3(N) = \prod_j \omega_{jk}^3 x_j^3(N) \\ &y_k^3(N) = f_k^3(net_k^3(N)) = net_k^3(N), \quad k = 1,\ldots, 9, \end{aligned} \tag{15}$$

where x_j^3 represents the jth input to the node of layer 3, ω_{jk}^3 represents the connected weights between the membership layer and the rule layer and is assumed to be unity, and k is the number of rules with complete rule connection if each input node has the same linguistic variables. In addition, in the output layer, the node input and the node output are denoted as

$$net_o^4(N) = \underset{k}{\ } \omega_{ko}^4 x_k^4, \quad y_o^4(N) = f_o^4(net_o^4(N)) = net_o^4(N), \quad o = 1, \tag{16}$$

where x_k^4 represents the kth input to the node of layer 4, and the connected weight ω_{ko}^4 represents the output action strength of the oth output associated with the kth rule.

In this study, the supervised gradient decent technique is adopted to derive the online algorithm of the WFNN. An error function E is defined as

$$E = \frac{1}{2}(\omega^*_{rm} - \omega_{rm})^2 = \frac{1}{2}e^2. \tag{17}$$

In the proposed WFNN, the connected weights of the output layer and the translation and dilation of the wavelet membership functions are trained online. The detailed derivation of the online learning algorithms based on the back-propagation method is similar to [9] and is omitted in this study. In addition, the online learning algorithms using varied learning-rate parameters can guarantee the convergence of the tracking error by using the convergence analysis of a discrete-type Lyapunov function. In the convergence analysis, the energy function E shown in (17) is represented as a discrete-type Lyapunov function. The resulting learning-rate parameter of the connected weights of the output layer η_ω is

$$\eta_\omega = \frac{E(N)}{4\left[\sum_k \left(\frac{\partial E(N)}{\partial y_1(k)}\frac{\partial y_1(k)}{\partial \omega_{k1}^4}\right)^2 + \varepsilon_0\right]}, \tag{18}$$

where ε_0 is a positive constant. Additionally, the resulted learning-rate parameters of the translation and dilation of the wavelet membership function η_a and η_b are as follows:

$$\eta_a = \frac{E(N)}{4\left[\sum_j \left(\frac{\partial E(N)}{\partial y_1(k)}\frac{\partial y_1(k)}{\partial net_j^2}\frac{\partial net_j^2}{\partial a_j}\right)^2 + \varepsilon_0\right]},$$
$$\eta_b = \frac{E(N)}{4\left[\sum_j \left(\frac{\partial E(N)}{\partial y_1(k)}\frac{\partial y_1(k)}{\partial net_j^2}\frac{\partial net_j^2}{\partial b_j}\right)^2 + \varepsilon_0\right]}. \tag{19}$$

Design and Experimentation

The specifications of the IPMSM are

- three-phase
- 945 W
- 6.87 A
- 2.25 N·m
- 4,000 r/min.

The insulated-gate bipolar transistor voltage source inverter with a switching frequency of 10 kHz is controlled by using SVPWM technology through the voltage vectors v_α^* and v_β^*, as shown in Figure 1. Moreover, the test platform of the IPMSM servo drive system comprises a torque meter, gear reducer, and magnetic powder brake. In addition, the implementation of the control algorithms for the IPMSM servo drive system is based on a TMS320F28075 32-b floating-point DSP with 120 MHz. The nominal value of the gains of the speed controller using the parameters of the IPMSM servo drive system, which are shown in Table 1, via the pole-zero cancellation technique are $K_P = 0.2$ and $K_I = 2$.

Table 1. The parameters of the IPMSM servo drive.

Items	Quantities	Items	Quantities
B	0.01216 N·m/(rad/s)	K_T	0.33081 N·m/A
K_q	82.24 (rad/s)/N·m	t_q	0.105 s
J	0.00128 N·m/(rad/s^2)	$t_{\Sigma D}$	0.0021 s

The simulation cutoff frequency Ω_b of the speed control loop of the IPMSM servo drive system is 21.2 Hz, as shown in Figure 4(a). The experimental frequency response of the speed control loop of the IPMSM servo drive system is shown in Figure 4(b), with the cutoff frequency Ω_b of 20.4 Hz, which is obtained by using an Agilent 35670 A dynamic signal analyzer. Owing to the uncertainties, including the damping of the IPMSM servo drive, the bandwidth of the experimental frequency response is smaller than the simulation frequency response. Since using the proposed WFNNs to tune the gains of the PI speed controller online makes the pole-zero cancellation fail, the closed-loop transfer function cannot be represented as a standard second-order transfer function. Thus, a third-order transfer function,

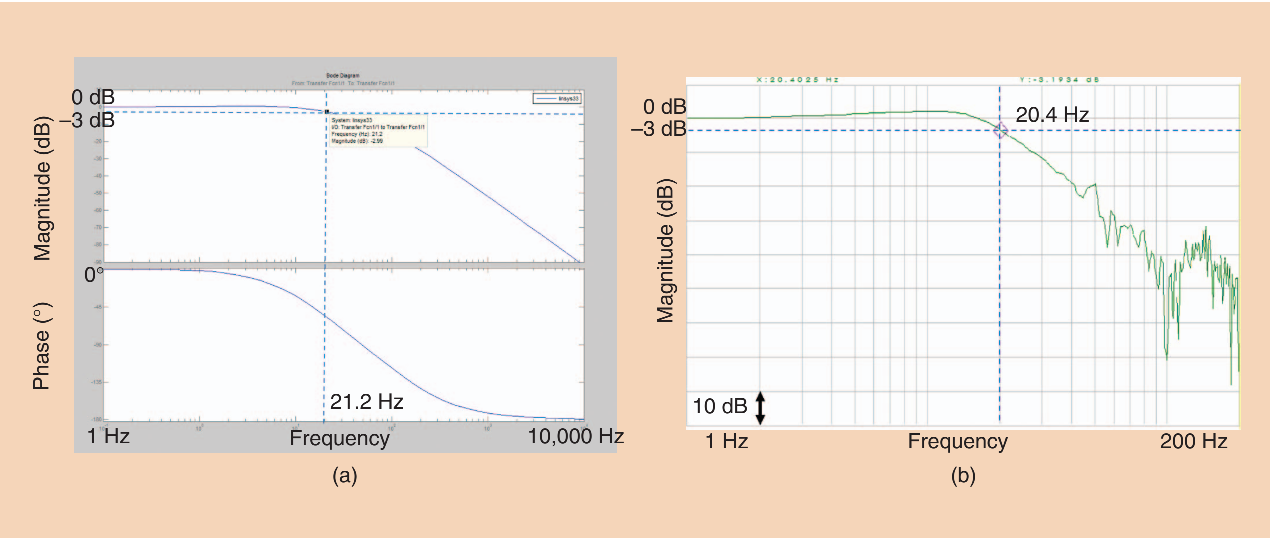

Figure 4. The test results of a nominal designed IPMSM servo drive system: the (a) simulation frequency response and (b) experimental frequency response.

considering the parameters of the IPMSM servo drive, results as follows:

$$G_c(s) = \frac{K_P K_T K_q t_i s + K_P K_T K_q}{t_i t_q T_{\Sigma D} s^3 + t_i (T_{\Sigma D} + t_q) s^2 + t_i (K_P K_T K_q + 1) s + K_P K_T K_q} = \frac{27.2 \frac{K_P^2}{K_I} s + 27.2 K_P}{0.0002205 \frac{K_P}{K_I} s^3 + 0.1071 \frac{K_P}{K_I} s^2 + (27.2 \frac{K_P^2}{K_I} + \frac{K_P}{K_I}) s + 27.2 K_P}. \quad (20)$$

In the experimentation, the sampling rates are 0.1 ms for the current control loop and 1 ms for the speed control loop. The execution or compute time of the C program in the TMS320F28075 32-b floating-point DSP can be obtained by the clock tool of the Texas Instruments Code Composer Studio version 5 program editing interface. The total operation cycles and total execution time for the WFNNs and FOC are 12,670 and 0.105 ms, respectively. As a result, the total execution time of the proposed online autotuning techniques using WFNNs is still less than 1 ms, which is the sampling interval of the speed control loop. Moreover, the searching mechanism for the proposed online autotuning technique using WFNNs is based on the rise time of different speed commands. According to the different rise times of 0.4, 0.3, and 0.2 s, a larger tracking error and its derivative will result in larger incremental values of K_P and K_I. And the undamped natural frequency Ω_n will increase accordingly.

The proposed online autotuning techniques using WFNNs can achieve the optimal bandwidth for the IPMSM servo drive according to the rise time of different speed commands at different load conditions.

Furthermore, according to (10), Ω_n is the main factor that is related to the –3-dB bandwidth. Therefore, the bandwidth of the speed control loop will be increased accordingly to achieve the optimal bandwidth for different rise times and to avoid overdesign of the bandwidth. In addition, in this study, the delay times of the current control loop, speed filter, and speed control loop are designed to be 0.0001, 0.001, and 0.001 s, respectively. All of the delay times of the speed control loop can be combined into an effective delay time $t_{\Sigma D}$, as shown in (3) and Table 1. Additionally, the parameters of the PI current controllers are tuned by trial and error to achieve the best transient and steady-state control performance, considering the stability requirement. The chosen parameters of the PI current controllers are $K_{iP} = 19$ and $K_{iI} = 2{,}000$, where K_{iP} and K_{iI} represent the proportional and integral gains of the PI current controllers, respectively.

Using the outputs of a standard second-order transfer function with rise times of 0.4, 0.3, and 0.2 s as three consecutive speed commands from 2,000 to 3,000 r/min at a no-load condition, the speed responses of the IPMSM servo drive system are shown in Figure 5(a). The current command i_q^* and speed-tracking error are shown in Figure 5(b). The outputs of the WFNNs ΔK_P and ΔK_I and the resulting PI speed controller gains are shown in Figure 5(c).

Furthermore, the simulation frequency responses of the speed control loop of the IPMSM servo drive system are shown in Figure 5(d)–(f) and are obtained by using (20) with the steady-state gains of the PI speed controller at the respective speed command. In addition, the experimental frequency responses of the speed control loop of the IPMSM servo drive system are shown in Figures 5(g)–(i) and are also obtained by using an Agilent 35670 A dynamic signal analyzer with the steady-state gains of the PI speed controller at the respective speed command. From the simulation frequency responses shown in Figure 5(d)–(f), the cutoff frequencies Ω_b are 23.2, 26.8, and 29.7 Hz, respectively. Additionally, from the experimentation frequency responses shown in Figure 5(g)–(i), the cutoff frequencies Ω_b are 20.9, 24.3, and 28.3 Hz, respectively. Therefore, the proposed online autotuning techniques using WFNNs can achieve the optimal bandwidth for the IPMSM servo drive according to the rise time of different speed commands.

Using the outputs of a standard second-order transfer function with rise times of 0.4, 0.3, and 0.2 s as three consecutive speed commands from 2,000 to 3,000 r/min at a 1-N·m load condition, the speed responses of the IPMSM servo drive system are shown in Figure 6(a), the speed-tracking error and current command i_q^* are detailed in Figure 6(b), and the outputs of the WFNNs ΔK_P and ΔK_I and the resulting PI speed controller gains are shown in Figure 6(c). Compared with the steady-state gains of the PI speed controller at a no-load condition, the gains are increased for the 1-N·m load condition to achieve the same rise time.

Furthermore, the simulation frequency responses of the speed control loop of the IPMSM servo drive system are included in Figure 6(d)–(f) and are obtained by using (20) with the steady-state gains of the PI speed controller at the respective speed command. In addition, the experimental frequency responses of the speed control loop of the IPMSM servo drive system are shown in Figure 6(g)–(i), with the steady-state gains of

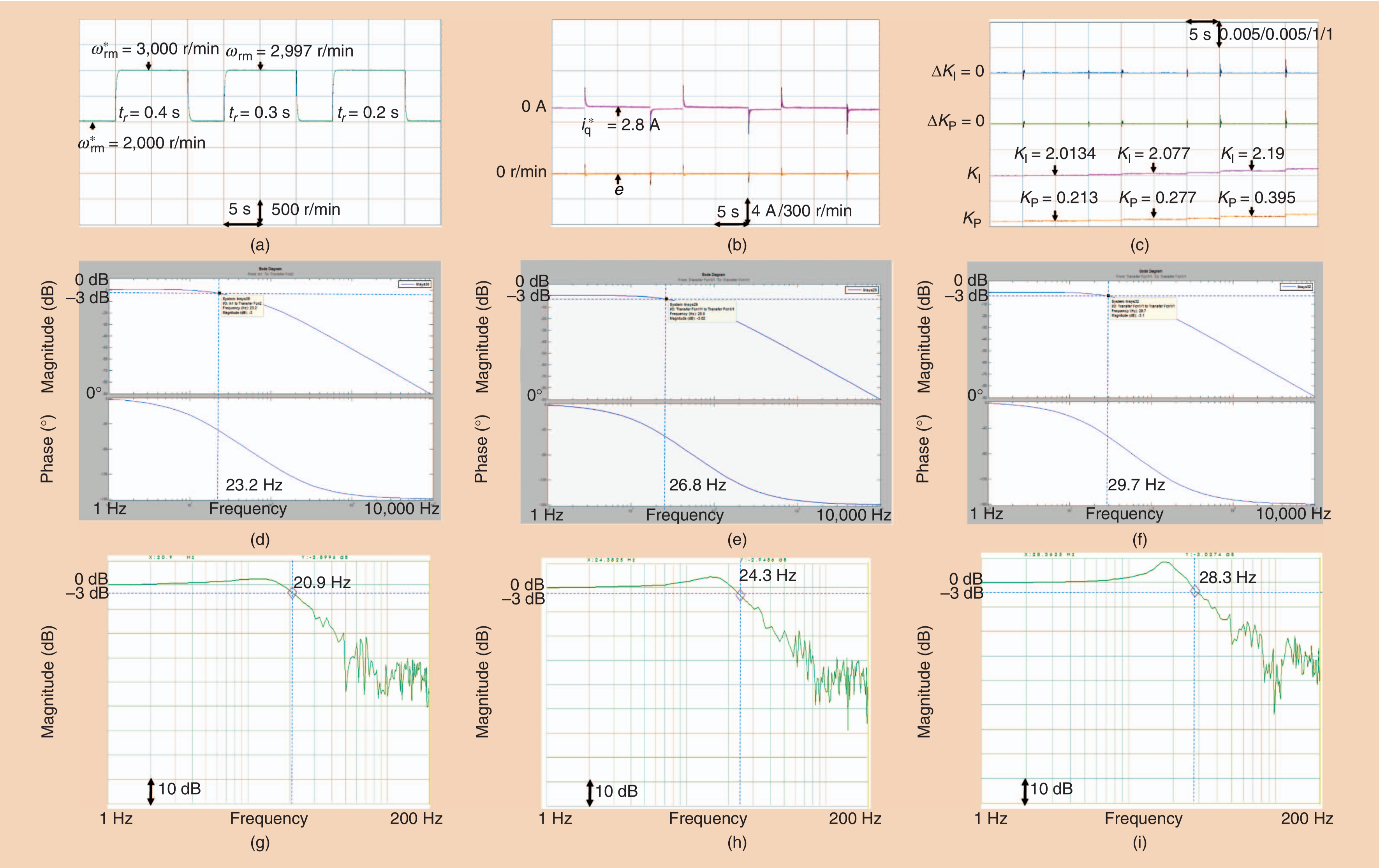

Figure 5. The test results of the online autotuning of a PI speed controller of an IPMSM servo drive system at no load: the (a) speed response at consecutive speed commands, (b) current command and tracking error, (c) outputs of the WFNNs and the resulting PI speed controller gains, (d) simulation frequency response at a rise time of 0.4 s, (e) simulation frequency response at a rise time of 0.3 s, (f) simulation frequency response at a rise time of 0.2 s, (g) experimental frequency response at a rise time of 0.4 s, (h) experimental frequency response at a rise time of 0.3 s, and (i) experimental frequency response at a rise time of 0.2 s. I/O: input-output.

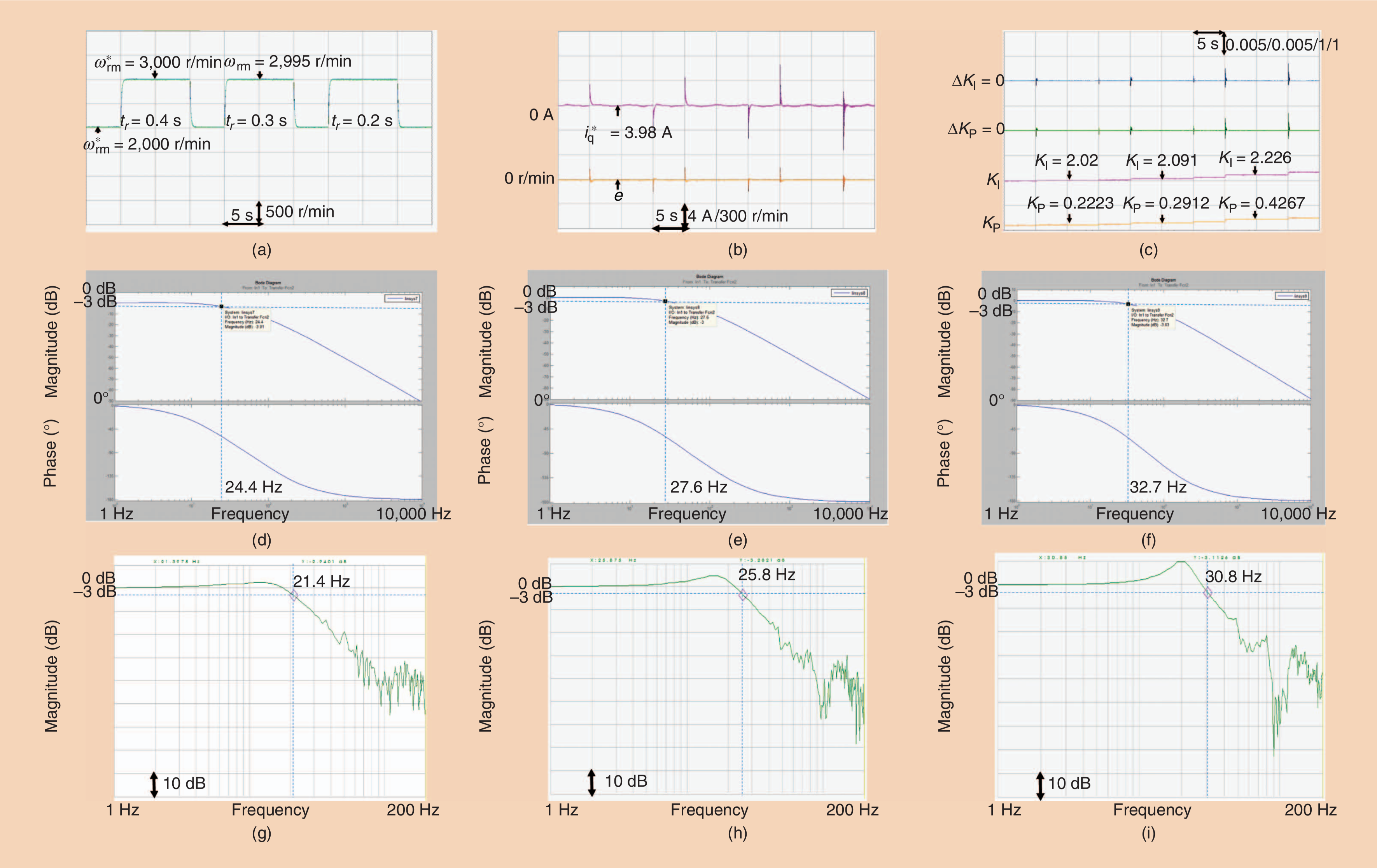

Figure 6. The test results of the online autotuning of a PI speed controller of an IPMSM servo drive system at a 1-N·m load: the (a) speed response at consecutive speed commands, (b) current command and tracking error, (c) outputs of the WFNNs and the resulting PI speed controller gains, (d) simulation frequency response at a rise time of 0.4 s, (e) simulation frequency response at a rise time of 0.3 s, (f) simulation frequency response at a rise time of 0.2 s, (g) experimental frequency response at a rise time of 0.4 s, (h) experimental frequency response at a rise time of 0.3 s, and (i) experimental frequency response at a rise time of 0.2 s.

the PI speed controller at the respective speed command. From the simulation frequency responses in Figure 6(d)–(f), the cutoff frequencies Ω_b are 24.4, 27.6, and 32.7 Hz, respectively. Additionally, from the experimentation frequency responses displayed in Figure 6(g)–(i), the cutoff frequencies Ω_b are 21.4, 25.8, and 30.8 Hz, respectively, which shows that the proposed online autotuning techniques using WFNNs can achieve the optimal bandwidth for the IPMSM servo drive according to the rise time of different speed commands at different load conditions.

The gains of the PI speed controller of the IPMSM servo drive were tuned automatically to achieve the required optimal bandwidth.

Conclusion

An intelligent autotuning scheme for the PI speed controller using two two-input, one-output, four-layer WFNNs was successfully developed and implemented in this study to achieve the optimal bandwidth of an FOC IPMSM servo drive. The proposed intelligent autotuning scheme was developed to search the optimal bandwidth of servo motor drives without using the information of plant parameters and the characteristics of servo motor drives. From the experimental results, the gains of the PI speed controller of the IPMSM servo drive were tuned automatically to achieve the required optimal bandwidth according to the rise time of different speed commands at different load conditions.

Acknowledgment

This work was supported by the National Science Council, Taiwan, through grant MOST 104-2221-E-008-040-MY3.

About the Authors

Faa-Jeng Lin (linfj@ee.ncu.edu.tw) earned his B.S. and M.S. degrees in electrical engineering from the National Cheng Kung University, Tainan, Taiwan, and his Ph.D. degree in electrical engineering from the National Tsing Hua University, Hsinchu City, Taiwan, in 1983, 1985, and 1993, respectively. Currently, he is the chair professor in the Department of Electrical Engineering at the National Central University, Taoyuan, Taiwan. He is an Institution of Engineering and Technology fellow, and he is a Fellow of the IEEE.

Shih-Gang Chen (csg12388@gmail.com) earned his B.S. degree in electrical engineering from Yuan Ze University, Taoyuan, Taiwan. He earned his M.S. degree in electrical engineering from the National Central University, Taoyuan, Taiwan, in 2016 and is currently working toward his Ph.D. degree.

Wei-An Yu (yusky1532@gmail.com) earned his B.S. degree in electrical engineering from the National Taiwan Ocean University, Keelung, Taiwan. He is currently working toward his M.S. degree in electrical engineering at the National Central University, Taoyuan, Taiwan.

Hsiao-Tse Chou (cht1674@gmail.com) earned his B.S. degree in electrical engineering from the National Chin-Yi University of Technology, Taichung, Taiwan. He is currently working toward his M.S. degree in electrical engineering at the National Central University, Taoyuan, Taiwan.

References

[1] J. Lemmens, P. Vanassche, and J. Driesen, "PMSM drive current and voltage limiting as a constraint optimal control problem," *IEEE J. Emerg. Sel. Topics Power Electron.*, vol. 3, no. 2, pp. 326–338, 2014.

[2] T. Sun, J. Wang, and X. Chen, "Maximum torque per ampere (MTPA) control for interior permanent magnet synchronous machine drives based on virtual signal injection," *IEEE Trans. Power Electron.*, vol. 30, no. 9, pp. 5036–5045, 2015.

[3] H. Wang, M. Yang, L. Niu, and D. Xu, "Current-loop bandwidth expansion strategy for permanent magnet synchronous motor drives," in *Proc. IEEE 5th Conf. Industrial Electronics and Applications*, 2010, pp. 1340–1345.

[4] J. Bocker, S. Beineke, and A. Bahr, "On the control bandwidth of servo drives," in *Proc. 13th European Conf. Power Electronics Applications*, 2009, pp. 1–10.

[5] C. J. Hsu and Y. S. Lai, "Novel on-line optimal bandwidth search and auto tuning techniques for servo motor drives," in *Proc. IEEE Energy Conversion Congr. and Exposition (ECCE)*, 2016, pp. 1–8.

[6] C. J. Hsu and Y. S. Lai, "Novel online optimal bandwidth search and auto tuning techniques for servo motor drives," *IEEE Trans. Ind. Appl.*, vol. 53, no. 4, pp. 3635–3642, 2017.

[7] F. J. Lin, H. J. Shieh, P. K. Huang, and L. T. Teng, "Adaptive control with hysteresis estimation and compensation using RFNN for piezo-actuator," *IEEE Trans. Ultrason., Ferroelect., Freq. Control*, vol. 53, no. 9, pp. 1649–1661, 2006.

[8] H. Pan and L. Z. Xia, "Efficient object recognition using boundary representation and wavelet neural network," *IEEE Trans. Neural Netw.*, vol. 19, no. 12, pp. 2132–2149, 2008.

[9] F. J. Lin, K. H. Tan, D. Y. Fang, and Y. D. Lee, "Intelligent controlled three-phase squirrel-cage induction generator system using wavelet fuzzy neural network for wind power," *IET Renew. Power Generat.*, vol. 7, no. 5, pp. 552–564, 2013.

[10] R. H. Abiyev and O. Kaynak, "Fuzzy wavelet neural networks for identification and control of dynamic plants: A novel structure and a comparative study," *IEEE Trans. Ind. Electron.*, vol. 55, no. 8, pp. 3133–3140, 2008.

[11] C. H. Lu, "Wavelet fuzzy neural networks for identification and predictive control of dynamic systems," *IEEE Trans. Ind. Electron.*, vol. 58, no. 7, pp. 3046–3058, 2011.

[12] W. Huang, S. K. Oh, and W. Pedrycz, "Fuzzy wavelet polynomial neural networks: Analysis and design," *IEEE Trans. Fuzzy Syst.*, vol. 25, no. 5, 2017.

[13] F. J. Lin and C. H. Lin, "A permanent-magnet synchronous motor servo drive using self-constructing fuzzy neural network controller," *IEEE Trans. Energy Convers.*, vol. 19, no. 1, pp. 66–72, 2004.

[14] F. J. Lin, R. J. Wai, and P. K. Huang, "Two-axis motion control system using wavelet neural network for ultrasonic motor drives," *IEE Proc.: Electr. Power Appl.*, vol. 151, no. 5, pp. 613–621, 2004.

SMC